


Photoconductive ZnO Films Printed on Flexible Substrates by Inkjet and Aerosol Jet Techniques

D.J. WINARSKI,¹ E. KREIT,² E.M. HECKMAN,² E. FLESBURG,¹
M. HASEMAN,¹ R.S. AGA,² and F.A. SELIM ^{1,3}

1.—Center for Photochemical Sciences, Bowling Green State University, Bowling Green, OH 43403, USA. 2.—Air Force Research Laboratory Sensors Directorate, Wright-Patterson Air Force Base, OH 45431, USA. 3.—e-mail: faselim@bgsu.edu

Zinc oxide (ZnO) thin films have remarkable versatility in sensor applications. Here, we report simple ink synthesis and printing methods to deposit ZnO photodetectors on a variety of flexible and transparent substrates, including polyimide (Kapton), polyethylene terephthalate, cyclic olefin copolymer (TOPAS), and quartz. X-ray diffraction analysis revealed the dependence of the film orientation on the substrate type and sintering method, and ultraviolet-visible (UV-Vis) absorption measurements revealed a band edge near 380 nm. van der Pauw technique was used to measure the resistivity of undoped ZnO and indium/gallium-codoped ZnO (IGZO) films. IGZO films showed lower resistivity and larger average grain size compared with undoped ZnO films due to addition of In³⁺ and Ga³⁺, which act as donors. A 365-nm light-emitting diode was used to photoirradiate the films to study their photoconductive response as a function of light intensity at 300 K. The results revealed that ZnO films printed by aerosol jet and inkjet techniques exhibited five orders of magnitude photoconductivity, indicating that such films are viable options for use in flexible photodetectors.

Key words: Flexible electronics, zinc oxide, photoconduction, UV photodetectors, aerosol jet printing, inkjet printing

INTRODUCTION

Printing electrically functional inks is more advantageous than conventional device fabrication due to its low cost and applicability for flexible devices. Aerosol jet printing (AJP) and inkjet printing (IJP) techniques are currently used to print a wide variety of organic and inorganic inks for use as flexible photodetectors, transistors, and other circuit board components.^{1–7} Recently, flexible ultraviolet (UV) photodetectors have attracted interest, as they are lightweight and can be feasibly conformed to an individual.^{8,9} Although organic-inorganic hybrids are being investigated,^{10,11} no significant work can be found on inorganic inks, which are expected to allow greater versatility of

printed materials for device applications, including for UV photodetection.

Zinc oxide (ZnO) has emerged as one of the most exciting materials for UV photodetection due to its direct, wide bandgap (3.2 eV at 298 K) and strong UV absorption.^{12,13} The electrical properties of ZnO can be tuned by addition of group II–IV metal ions.¹⁴ Sol-gel techniques can easily be used to fabricate ZnO films at low cost,¹⁵ making it suitable for use in flexible devices.

Additive manufacturing techniques, such as IJP and AJP, allow effective development of high-performance patterned ZnO devices at low cost. ZnO-based inks have already been printed for use in UV photodetectors,¹⁶ transistors,^{17,18} or seeding layers.¹⁹ Recently, Tran et al. reported deposition of a precursor solution on Kapton substrate via IJP to fabricate flexible ZnO UV photodetectors,²⁰ but we are not aware of any reports on AJP of ZnO.

Table I. Summary of ZnO films printed and studied in this work, with substrate type, printing method, and sintering conditions

Sample	Substrate	Printing method	Sintering conditions
ZnO ¹	TOPAS	Inkjet	170°C, 60 min
ZnO ²	Kapton	Inkjet	300°C, 20 min
ZnO ³	TOPAS	Inkjet	Xenon, 180 bursts
ZnO ³	Kapton	Inkjet	Xenon, 180 bursts
ZnO ³	PET	Inkjet	Xenon, 180 bursts
ZnO ⁴	TOPAS	Inkjet	150°C, 30 min
ZnO ⁴	Kapton	Inkjet	150°C, 30 min
ZnO ⁵	Kapton	Inkjet	400°C, 60 min
ZnO ⁶	Kapton	Aerosol Jet	200°C, 60 min
ZnO ⁷	Kapton	Aerosol Jet	300°C, 60 min
ZnO ⁸	Kapton	Aerosol Jet	400°C, 60 min
IGZO	Quartz	Inkjet	400°C, 60 min
IGZO	Kapton	Inkjet	400°C, 60 min
IGZO	Kapton	Aerosol Jet	400°C, 60 min

In this work, we fabricated ZnO photodetectors by preparing simple sol-gel inks and depositing them onto flexible substrates using IJP and AJP techniques. Inks were made by dissolving zinc salt into a solvent with stabilizer, and some inks were doped with In³⁺ and Ga³⁺ ions in solution to increase the overall electrical conductivity. Inkjet and aerosol jet printers were used to deposit square patterns of ink, followed by various sintering processes to form ZnO wurtzite structure. Ultraviolet-visible (UV-Vis) analysis was used to confirm the bandgap (~3.2 eV) of ZnO and examine the quality of the printing and sintering processes. X-ray diffraction (XRD) measurements were performed on films produced by IJP and AJP to investigate the effects of the substrate and sintering processes on the ZnO structure, as well as the effects of the In³⁺ and Ga³⁺ dopants on the grain size. Ohmic silver contacts were printed on some ZnO films using an aerosol jet printer to carry out van der Pauw measurements with and without illumination at 365 nm. These measurements revealed that the printed ZnO films were highly photoconductive, indicating their great potential for use in development of flexible photodetectors.

EXPERIMENTAL PROCEDURES

Zinc Oxide Precursor Ink Synthesis

Inks were made using 2-methoxyethanol (99.8%, Sigma-Aldrich) and ethanolamine (99%, Acros Organics) as solvent and stabilizer, respectively. Zinc acetate (99.99%, Sigma-Aldrich) was dissolved at 1:1 molar ratio with ethanolamine to obtain 0.75 M precursor solution. Solutions were prepared in open-air environment, then covered with plastic paraffin film, heated to 60°C and magnetically stirred for 2 h to obtain transparent homogeneous solution. Indium/gallium-codoped ZnO (IGZO) precursor solutions were made at the same molar ratios and concentrations by replacing some zinc acetate

with gallium(III) nitrate hydrate (99.9998%, Acros Organics) and indium(III) acetate hydrate (99.99%, Sigma-Aldrich) to obtain a Zn:In:Ga ratio of 98:1:1. These inks were printed within a week of synthesis; no precipitate formation or color change was observed before or after doping.

Printing and Curing Zinc Oxide Patterns

Inks were used to print 7 mm × 7 mm square patterns on polyimide (Kapton), cyclic olefin copolymer (TOPAS), polyethylene terephthalate (PET), and quartz, using IJP and AJP techniques. Substrates were prepared by swabbing with acetone and isopropanol, drying with a nitrogen gun, and applying atmospheric plasma treatment from a corona discharge wand with the transformer set at 200 W at standoff distance of 5 mm from the ground electrode. A Dimatix inkjet printer was used to print 12 layers of ZnO or IGZO ink with at least 50% droplet overlap and jet and platen temperatures set to 39°C. Droplet size ranged from 50 μm to 100 μm depending on the substrate. Printed inks were dried at 150°C for 10 min to 30 min (until visibly dry) to remove solvent. Thermal sintering was carried out in ambient on a hot plate set between 170°C and 400°C for 20 min to 60 min. Photonic sintering was carried out in a nitrogen-rich atmosphere using a xenon arc lamp placed 4.445 cm above the substrate platen, set at 2 kV with 6 ms pulse width for a total of 180 bursts. An Optomec aerosol jet printer was used to print six layers of ZnO ink onto Kapton substrates at 3 mm/s nozzle speed in a 50-μm serpentine pattern. The line width of the aerosol spray was about 75 μm. These inks were dried at 90°C for 30 min (until visibly dry), then subject to thermal sintering at 200°C, 300°C, and 400°C for 1 h. The drying times and sintering temperatures for the IJP and AJP ZnO films varied because of the line overlap of the printed ZnO patterns and the melting point of each substrate. Table I lists the

ZnO samples and their printing methods and sintering conditions. ZnO¹ thru ZnO⁸ refer to different sintering conditions.

Printing of Silver Contacts

Silver inks have been widely used to print electrodes because of their low sintering temperature and high electrical conductivity. Commercial silver ink from Clariant was printed as 1.5 mm × 1.5 mm square patterns using the aerosol jet printer. The electrodes overlapped a 0.7 mm × 0.7 mm area of each corner of the ZnO squares. Silver ink was only printed on ZnO films that were cured above 200°C (ZnO⁵ to ZnO⁸ and IGZO) to limit the effect of this additional thermal treatment on the films. The silver ink was dried at 90°C for 30 min, then at 180°C for 60 min. Ohmic contact resistance was confirmed before carrying out van der Pauw measurements.

Characterization of Printed Zinc Oxide Films

Absorbance spectra of ZnO films were recorded using a dual-beam PerkinElmer UV–Vis spectrometer. A blank substrate was placed in line with the reference beam while the ZnO sample spectra were recorded. Film crystallinity was studied using a Rigaku x-ray diffractometer to determine the ZnO crystal phase (*hkl* values) and average grain size. At 300 K, the resistivity as a function of light intensity was obtained via van der Pauw measurements using an MMR Hall-effect system equipped with a 365-nm light-emitting diode (LED), positioned 1.8 cm from the sample stage. Before illumination, dark measurements were taken, then the LED light intensity was increased in steps up to 24 mW ($\sim 4.4 \times 10^{16}$ photons/cm² s), allowing the light and temperature to stabilize for at least 1 min prior to each measurement. Although light from the LED produces localized heating, the temperature was maintained at 300 K using a Joule–Thompson refrigerator located directly beneath the sample stage, operating in combination with a heating element to balance the temperature.

RESULTS AND DISCUSSION

Optical and Structural Characterization

The band edge of ZnO at 380 nm was clearly seen in the absorbance spectra. Figure 1 shows the absorbance of different printed ZnO films. The bandgap was about 3.2 eV, as calculated for each film from a Tauc plot for direct-bandgap transitions, as shown in Fig. 2, which shows a linear fit for each $(\alpha h\nu)^2$ curve. AJP IGZO films exhibited higher transparency than IJP films regardless of the sintering conditions applied, due to light scattering from surface roughness and striations in the IJP films. As expected, AJP yielded much higher quality than IJP, as was apparent to the naked eye. Figure 3 shows IJP and AJP films printed on

Kapton and sintered at 300°C. Furthermore, the effect of photonic sintering by xenon arc lamp versus thermal sintering for ZnO IJP films on TOPAS is compared in Fig. 1. ZnO³, which was sintered using the xenon arc lamp, was more transparent than ZnO¹, which was sintered using a hot plate at 170°C.

XRD analysis was applied to determine the ZnO structure of various IJP ZnO films. The results are shown in Fig. 4, where all ZnO (*hkl*) crystal phases are labeled. ZnO phases form at temperatures as low as 150°C, and more peaks appear as the sintering temperature increases above 150°C. Interestingly, we observed formation of ZnO phases for ZnO⁴ on TOPAS, but not for ZnO⁴ on Kapton, which could be due to the minimal sintering time or thicker substrate in the latter case. In addition, an impurity phase could be seen in the pattern for ZnO³ on TOPAS. Despite this, the results of these measurements demonstrate successful printing and sintering processes for ZnO thin films.

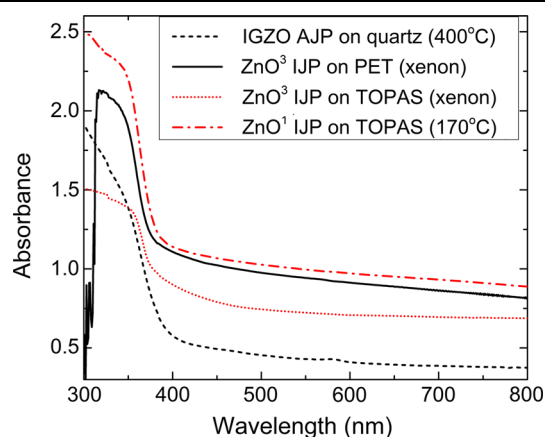


Fig. 1. UV–Vis absorbance spectra for IJP and AJP ZnO films sintered by different methods, exhibiting band edge near 380 nm.

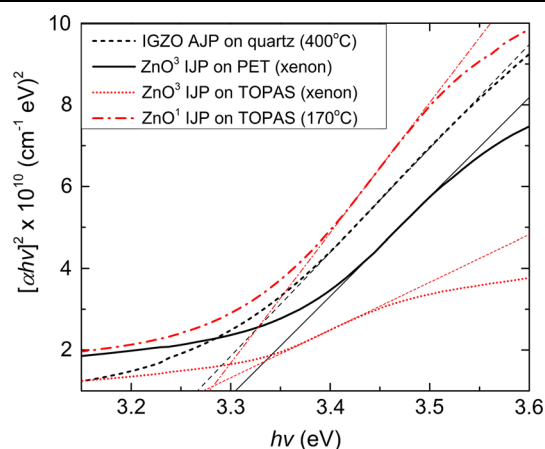


Fig. 2. Tauc plots of direct-bandgap transitions for absorbance spectra shown in Fig. 1, with linear fit extrapolated to $(\alpha h\nu)^2 = 0$ for bandgap determination of each curve.

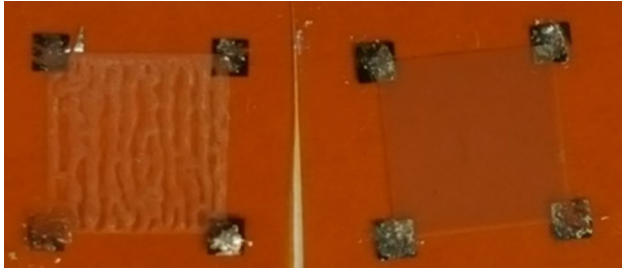


Fig. 3. Comparison of ZnO thin films printed by IJP (left) and AJP (right) sintered at 300°C.

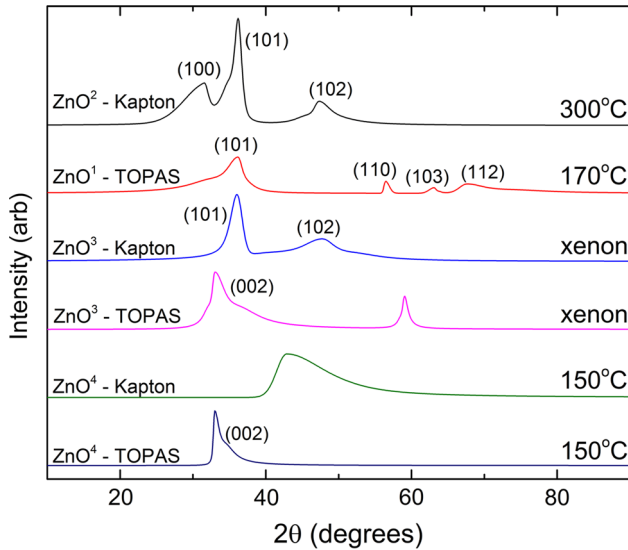


Fig. 4. X-ray diffraction spectra for IJP inks on Kapton and TOPAS substrates sintered by hot plate and xenon arc lamp.

In Fig. 5, the XRD patterns for AJP ZnO reveal formation of ZnO with wurtzite structure as a function of temperature. No peaks characteristic of In_2O_3 or Ga_2O_3 were found. The films showed amorphous nature at 200°C, with slight alignment in (101) orientation, and became more polycrystalline as the annealing temperature was increased. The average grain size increased with the sintering temperature, consistent with previous reports on structural characterization of sol-gel-derived ZnO thin films.^{21,22} The AJP IGZO XRD results revealed ZnO patterns similar to those for undoped ZnO, as the same crystal phases formed in the ZnO^8 and IGZO films when printed on Kapton substrate and sintered under the same conditions; however, the average grain size was much larger for the IGZO films. The low doping concentration of In^{3+} and Ga^{3+} had a minimal effect on the phase orientation of the ZnO structure, but increased the average grain size by about 50%. This is inconsistent with findings that In^{3+} and Ga^{3+} dopants create amorphous phases of In_2O_3 or Ga_2O_3 and decrease the average grain size,²³ but we are unaware of reports on the structural effects of these dopants in sol-gel ZnO

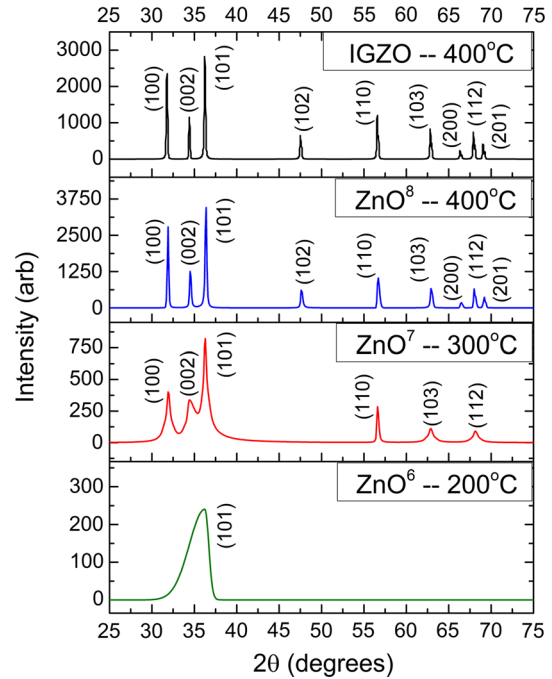


Fig. 5. X-ray diffraction spectra for AJP ZnO films on Kapton sintered at 200°C, 300°C, and 400°C and AJP IGZO films on Kapton sintered at 400°C.

inks for AJP. Table II lists the average grain size for AJP ZnO and IGZO films sintered under different conditions. The grain size D was calculated for each θ peak using the Scherrer equation

$$D = 0.9\lambda/\beta \cos \theta, \quad (1)$$

where $\lambda = 1.54 \text{ \AA}$ is the x-ray wavelength, β is the full-width at half-maximum (FWHM) of the corresponding peak, and θ is the Bragg angle.

Our homemade ZnO and IGZO precursor inks were successfully printed to form ZnO using both the IJP and AJP techniques. The growth orientation depended on the substrate type, while the printing and sintering processes significantly affected the structural and optical properties of the resulting film. Furthermore, incorporation of In^{3+} and Ga^{3+} dopants into the solution effectively increased the average grain size without inhibiting ZnO wurtzite formation.

Photoconductivity

Photoconductivity was observed by measuring the resistivity of IJP ZnO^5 , IJP IGZO, and AJP ZnO films as a function of light intensity at 365 nm. The average thickness of the films, measured using a stylus profilometer, was then used to calculate the resistivity, as summarized in Fig. 6.

The effect of In^{3+} and Ga^{3+} addition was investigated by comparing IJP IGZO and ZnO^5 films, both on Kapton with average thickness of 600 nm. As anticipated, IJP IGZO exhibited lower resistivity ($3.06 \times 10^4 \text{ } \Omega \text{ cm}$) than IJP ZnO ($4.59 \times 10^5 \text{ } \Omega \text{ cm}$),

Table II. Average grain size and standard error values, calculated by Scherrer equation, for ZnO and IGZO printed by AJP

Sample	Sintering condition	Average grain size (Å)	Estimated standard deviation (ESD)
ZnO ⁶	200°C, 60 min	32.33	6.04
ZnO ⁷	300°C, 60 min	239.17	36.25
ZnO ⁸	400°C, 60 min	500.32	119.91
IGZO	400°C, 60 min	736.84	27.85

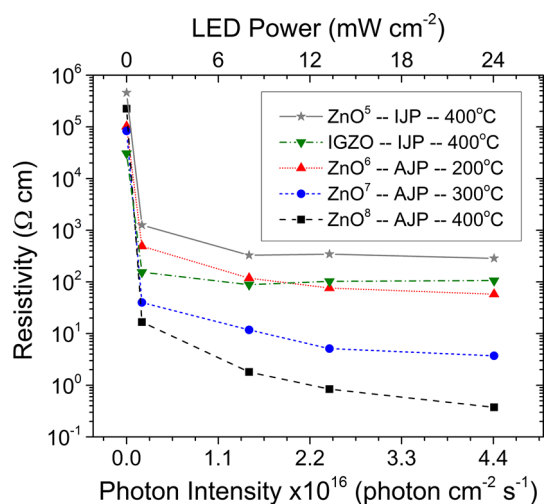


Fig. 6. Van der Pauw resistivity measurements of ZnO films as function of light intensity (365 nm LED).

an effect that has been seen in other sol-gel-prepared In- and Ga-doped ZnO thin films.^{24,25} IJP IGZO also exhibited lower resistivity than all AJP ZnO films. Furthermore, we observed a sharp decrease in resistivity by a factor of 100 for both IJP ZnO⁵ and IJP IGZO films after initial UV LED illumination at 0.98 mW ($\sim 1.8 \times 10^{15}$ photons/cm² s) due to valence to conduction band excitation from light absorption. This well-known process occurs because UV photons have greater energy (~ 3.4 eV) than the bandgap of ZnO films (~ 3.2 eV). Once illuminated, the photodetectors quickly saturated, as the resistivity remained relatively constant with increasing light intensity.

AJP ZnO films (all with thickness of 400 nm \pm 10%) were also tested for photoconductivity. Dark measurements showed that ZnO⁷, which was annealed at 300°C, exhibited lower resistivity (8.36×10^4 Ω cm) than ZnO⁶ (1.02×10^5 Ω cm) and ZnO⁸ (2.25×10^5 Ω cm), which were annealed at 200°C and 400°C, respectively. As generally reported, the resistivity of the ZnO thin films increased with increasing annealing temperature.^{26,27} However, low-temperature sintering of sol-gel-deposited ZnO films shows the opposite effect, with the lowest resistivity value achieved

when annealing at 300°C, as reported in Ref. 28. The overall resistivity depends on the structural properties of the ZnO, which are affected by introduction of oxygen through ambient thermal sintering. During the sintering process, increasing the temperature will first remove the solvent then continue to form ZnO phase and increase the average grain size, creating conductive pathways and consequently decreasing the resistivity. Once the solvent has been removed, higher sintering temperatures does not only further increase the average grain size in the film, but also increases the oxygen concentration. Increasing the grain size would decrease the resistivity,²⁹ while introducing more oxygen may increase the resistivity,³⁰ resulting in a local minimum in the resistivity as a function of sintering temperature.

Like IJP ZnO⁵ and IJP IGZO films, AJP ZnO films are photoconductive due to the valence to conduction band excitation from the 365-nm photons. In fact, there was an initial decrease in resistivity by a factor of at least 100, 1000, and 10,000 for the AJP ZnO⁶, ZnO⁷, and ZnO⁸ films, respectively. The photoconductive response of porous AJP ZnO films may be due to oxygen adsorption into the film. Upon light illumination, oxygen desorbs and releases trapped electrons to the conduction band, decreasing the resistivity.³¹ Therefore, the greatest photoresponse corresponding to the highest sintering temperature could be due to larger grains adsorbing more oxygen and, thus, releasing a greater number of electrons when illuminated. In addition, the lower grain-boundary density would allow for better electron mobility and greater photocurrent.

As the UV illumination was increased, a decrease in resistivity was observed for AJP ZnO films. With increasing light intensity, photogenerated holes can be trapped at charged boundary states, decreasing the barrier, and excess electrons can be promoted to the conduction band, increasing the free carriers. In addition to the charge state of the grain boundary, defect charge states may also change upon illumination. A charge at a defect could increase electron scattering, decreasing the electron mobility and compromising the conductivity. Both the carrier concentration and mobility affect the electrical properties of ZnO thin films, and different photoinduced processes could lead to the observed nonlinear behavior with increasing light intensity.

CONCLUSIONS

A facile ink formula was used to fabricate photoconductive ZnO films on flexible substrates via IJP and AJP techniques. Ohmic contact pads were made with commercial silver inks for reliable van der Pauw measurements. Evidence for successful printing of sol-gel ZnO onto flexible or transparent substrates was provided by UV-Vis spectroscopy and XRD analysis of IJP inks. Increasing the sintering temperature enhanced formation of ZnO phase and led to an increase in the average grain size of AJP films. Addition of In^{3+} and Ga^{3+} also increased the average grain size and enhanced the electrical conductivity of AJP and IJP films. AJP produced higher-quality ZnO films than IJP, and the data revealed five orders of magnitude photoconductivity with no saturation for AJP films. This study shows that it is possible to develop ZnO for flexible photodetectors and other flexible devices and reveals the great potential of ZnO for use in printronic technology.

ACKNOWLEDGEMENTS

The authors thank Dayton Area Graduate Studies Institute (DAGSI) for funding this work.

CONFLICT OF INTEREST

The authors declare that they have no conflicts of interest.

REFERENCES

1. L. Teng, M. Plötner, A. Türke, B. Adolphi, A. Finn, R. Kirchner, and W.J. Fischer, *Microelectron. Eng.* 110, 292 (2013).
2. Y. ZhouPing, H. YongAn, B. NingBin, W. XiaoMei, and X. YouLun, *Chin. Sci. Bull.* 55, 3383 (2010).
3. M.G. Mohammed and R. Kramer, *Adv. Mater.* 29, 1604965 (2017).
4. Y.F. Liu, W.S. Hwang, Y.F. Pai, and M.H. Tsai, *Microelectron. Reliab.* 52, 391 (2012).
5. R. Eckstein, T. Rödlmeier, T. Glaser, S. Valouch, R. Mauer, U. Lemmer, and G. Hernandez-Sosa, *Adv. Electron. Mater.* 1, 1500101 (2015).
6. R.S. Aga, J.P. Lombardi, C.M. Bartsch, and E.M. Heckman, *IEEE Photonic Technol. Lett.* 26, 305 (2013).
7. J.P. Lombardi, R.S. Aga, E.M. Heckman, and C.M. Bartsch, *Electron. Lett.* 50, 778 (2015).
8. J. Han, J. Lee, and A. Ju, *AIP Adv.* 6, 045218 (2016).
9. C. Zhou, X. Wang, X. Kuang, and S. Xu, *J. Micromech. Microeng.* 26, 075003 (2016).
10. X. Wang, W. Song, B. Liu, G. Chen, D. Chen, C. Zhou, and G. Shen, *Adv. Funct. Mater.* 23, 1202 (2013).
11. Z. Lou and G. Shen, *Adv. Sci.* 3, 1500287 (2016).
12. E. Monroy, F. Omnès, and F. Calle, *Semicond. Sci. Technol.* 18, R33 (2003).
13. Ü. Özgür, Y.I. Alivov, C. Liu, A. Teke, M.A. Reshchikov, S. Doğan, V. Avrutin, S.J. Cho, and H. Morkoç, *J. Appl. Phys.* 98, 041301 (2005).
14. A. Janotti and C.G. Van de Walle, *Rep. Prog. Phys.* 72, 126501 (2009).
15. D.J. Winarski, W. Anwand, A. Wagner, P. Saadatkia, F.A. Selim, M. Allen, B. Wenner, K. Leedy, J. Allen, S. Tetlak, and D.C. Look, *AIP Adv.* 6, 095004 (2016).
16. X. Liu, L. Gu, Q. Zhang, J. Wu, Y. Long, and Z. Fan, *Nat. Commun.* 5, 4007 (2014).
17. K. Everaerts, L. Zeng, J.W. Hennek, D.I. Camacho, D. Jariwala, M.J. Bedzyk, M.C. Hersam, and T.J. Marks, *ACS Appl. Mater. Interfaces* 5, 11884 (2013).
18. Y.Y. Noh, X. Cheng, H. Sirringhaus, J.I. Sohn, M.E. Welland, and D.J. Kang, *Appl. Phys. Lett.* 91, 043109 (2007).
19. Y.N. Liang, B.K. Lok, L. Wang, C. Feng, A.C.W. Lu, T. Mei, and X. Hu, *Thin Solid Films* 544, 509 (2013).
20. V.T. Tran, Y. Wei, H. Yang, Z. Zhan, and H. Du, *Nanotechnology* 28, 095204 (2017).
21. A.B. Yadav, C. Periasamy, S. Jit, and I.O.P. Conf, *Ser. Mater. Sci.* 73, 012060 (2015).
22. E. López-Mena, S. Jiménez-Sandoval, and O. Jiménez-Sandoval, *J. Sol Gel Sci. Technol.* 74, 419 (2015).
23. N. Vorobyeva, M. Rumyantseva, D. Filatova, F. Spiridonov, V. Zaytsev, A. Zaytseva, and A. Gaskov, *Chemosensors* 5, 18 (2017).
24. R. Bel-Hadj-Tahar and A.B. Mohamed, *New J. Glass Ceram.* 4, 55 (2014).
25. K. Nayak, J. Yang, J. Kim, S. Chung, J. Jeong, C. Lee, and Y. Hong, *J. Appl. Phys. D Appl. Phys.* 42, 035102 (2009).
26. M. Ashgar, H. Noor, M.S. Awan, S. Naseem, and M. Hasan, *Mater. Sci. Semicon. Proc.* 11, 30 (2008).
27. N. Bouhssira, S. Abed, E. Tomasella, J. Cellier, A. Mosbah, M.S. Aida, and M. Jacquet, *Appl. Surf. Sci.* 252, 5594 (2006).
28. S.S. Shariffudin, M.H. Mamat, S.H. Herman, and M. Rusop, *J. Nanomater.* 2012, 359103 (2012).
29. M.I. Khan, K.A. Bhatti, R. Qindeel, N. Alonizan, and H.S. Althobaiti, *Results Phys.* 7, 651 (2017).
30. N.R. Aghamalyan, I.A. Gambaryan, EKh Goulanian, R.K. Hovsepian, R.B. Kostanyan, S.I. Petrosyan, E.S. Vardanyan, and A.F. Zerrouk, *Semicond. Sci. Technol.* 18, 525 (2003).
31. Y. Takahashi, M. Kanamori, A. Kondoh, H. Minoura, and Y. Ohya, *Jpn. J. Appl. Phys.* 33, 6611 (1994).